中国光学 Chinese Optics 核心期刊

双波长窄带宽介质超材料吸收器

方晓敏 江孝伟 武华

Dual-wavelength narrow-bandwidth dielectric metamaterial absorber

FANG Xiao-min, JIANG Xiao-wei, WU Hua

引用本文:
方晓敏, 江孝伟, 武华. 双波长窄带宽介质超材料吸收器[J]. 中国光学, 2021, 14(6): 1327−1340. doi: 10.37188/CO.2021−0075
FANG Xiao-min, JIANG Xiao-wei, WU Hua. Dual-wavelength narrow-bandwidth dielectric metamaterial absorber[J]. *Chinese Optics*, 2021, 14(6): 1327-1340. doi: 10.37188/CO.2021-0075

在线阅读 View online: https://doi.org/10.37188/CO.2021−0075

文章编号 2095-1531(2021)06-1327-14

Dual-wavelength narrow-bandwidth dielectric metamaterial absorber

FANG Xiao-min[1], JIANG Xiao-wei[1*], WU Hua[2]
(1. *Faculty of Information Engineering*, *Quzhou College of Technology*, *Quzhou* 324100, *China*;
2. *College of Physics and Electronic Information*, *Gannan Normal University*, *Ganzhou* 341000, *China*)
* *Corresponding author*, *E-mail*: *JosephJiangquzhi*@126.*com*

Abstract: In order to reduce the manufacturing cost of the narrow-bandwidth Metamaterial Absorber (MA) and broaden its application field, a dual-wavelength dielectric narrow-bandwidth MA, composed of Au substrate, SiO_2 dielectric layer and Si dielectric asymmetric grating, is designed based on the finite-difference time-domain method using dielectric materials. It is found by simulation that the proposed narrow-bandwidth MA has ultra-high absorption efficiency at λ_1 = 1.208 52 μm and λ_2 = 1.238 21 μm, and the FWHM is only 0.735 nm and 0.077 nm, respectively. The main principle that MA achieves the narrow-bandwidth absorption at λ_1 is mainly due to the formation of Fabry-Pérot (FP) cavity resonance in the SiO_2 layer, while the narrow-bandwidth absorption of MA at λ_2 is mainly due to the guided mode resonance effect of the incident light in the asymmetric grating. The theoretical calculations show that the absorption characteristics can be affected more significantly by changing the structural parameters of the MA.

Key words: metamaterial absorber; dual-wavelength; narrow-bandwidth; Fabry-Pérot cavity resonance; guided mode resonance

双波长窄带宽介质超材料吸收器

方晓敏[1], 江孝伟[1*], 武 华[2]
(1. 衢州职业技术学院 信息工程学院, 浙江 衢州 324100;
2. 赣南师范大学 物理与电子信息学院, 江西 赣州 341000)

摘要: 为降低窄带宽超材料吸收器(Metamaterial Absorber, MA)制造成本的同时拓宽其应用领域, 本文基于时域有限差分法利用介质材料设计出双波长窄带宽介质 MA, 其由 Au 衬底、SiO_2 介质层和 Si 介质非对称光栅构成。经模拟计算发现, 本文提出的双波长窄带宽介质 MA 在 λ_1=1.208 52 μm 和 λ_2=1.238 21 μm 具有超高吸收效率, 而且 FWHM 也分别只有 0.735 nm 和 0.077 nm。MA 在 λ_1 实现窄带宽吸收主要是因为光在 SiO_2 层形成了法布里-珀罗 (Fabry-Pérot, FP) 腔共

收稿日期: 2021-04-13; **修订日期:** 2021-05-11

基金项目: 国家自然科学基金 (No. 61575008, No. 61650404)、江西省自然科学基金(No. 20171BAB202037)、江西省教育厅科技项目 (No. GJJ170819)、衢州市科技计划项目 (No. 2019K20)
Supported by National Natural Science Foundation of China (No. 61575008, No. 61650404), Jiangxi Natural Science Foundation (No. 20171BAB202037), Technology Project of Jiangxi Provincial Education Department (No. GJJ170819), Quzhou Science and Technology Project (No. 2019K20)

振，而 MA 在 λ_2 实现窄带宽吸收主要是由于入射光在介质非对称光栅中形成了导模共振效应。经理论计算可知，通过改变 MA 的结构参数可对其吸收特性产生较为显著的影响。

关　键　词: 超材料吸收器；双波长；窄带宽；法布里-珀罗腔共振；导模共振
中图分类号: TN256　　**文献标志码:** A　　**doi:** 10.37188/CO.2021-0075

1 Introduction

Perfect absorption of electromagnetic waves is required in many applications, such as solar cells, thermal emitters, radiation cooling, communication[1-4]. However, the absorbers made of natural materials can lead to impedance mismatch due to the lack of magnetic response, and therefore they cannot completely suppress light reflection, thus reducing the light absorption capacity of the absorber[5]. Therefore, metamaterial-based absorbers have been proposed, and because the Metamaterial Absorber (MA) has high absorption efficiency for electromagnetic wave, and has the advantages of compact size and settable operating wavelength, it is gradually gaining attention and becoming one of the research hotspots[6].

With further in-depth research, different types of MA have been gradually designed and fabricated, such as wide-bandwidth MA, narrow-bandwidth MA, terahertz MA, and tunable MA[7-9]. The reason why narrow-bandwidth MAs have received attention is that narrow-bandwidth MAs are more efficient in detection and thermal emitters compared to wide-bandwidth MAs[10-11], and only narrow-bandwidth in optical modulation, optical detection, and tailoring of thermal radiation MA can meet the requirements[12-13]. Different structures of narrow-bandwidth MA have been proposed, such as narrow-bandwidth MA based on Split Ring Resonator (SRR) arrays, metal/dielectric periodic gratings, and metal/dielectric slits (narrow slits). In 2014, Min Qiu et al. (KTH Royal Institute of Technology) proposed etching metal grating on a silver (Ag) metal substrate, and based on the surface plasmon excitonic resonance formed by Ag grating and air medium they successfully enabled MA with narrow-bandwidth absorption at wavelength 1 400 nm, and its linewidth(FullWidthHalfMaximum,FWHM)canreach 0.4 nm[14]; in 2018, FENG A et al. (the Chinese University of Hong Kong) proposed a narrow-bandwidth MA consisting of asymmetric metal grating and metal substrate, and a SiO_2 transition layer was added between the grating and the substrate, and the narrow-bandwidth MA was found to achieve ultra-narrow absorption in the optical communication band with a FWHM of 0.28 nm[15]; In 2019, KANG S et al. (Southeast University) proposed to etch a cross-shaped nanoarray composed of gold (Au) on a silicon dioxide substrate, while growing a thin layer of Au on the other side of the silicon dioxide to suppress transmission, and the MA was tested and found to achieve narrow-bandwidth absorption in the terahertz band[16].

From the above, it can be found that the materials used in the micro-nano structures in these narrow-bandwidth MAs are metallic materials, but metallic materials have ohmic losses and there are processing problems for fine metallic materials at high frequencies, both of which will affect the application promotion of MAs in the future to some extent. For this reason, some research groups have proposed to design and fabricate narrow-bandwidth MAs using dielectric materials. In 2019, Zhibin Ren et al. (Harbin Institute of Technology) designed and prepared MAs with narrow-bandwidth absorption in the infrared band using silicon nitride and indium tin oxide materials, which were tested to have a FWHM of up to 2.6 nm[17]; in 2020, Yan Zhao et al. (Anhui University) proposed a dielectric grating composed of silicon material etched directly on a metal substrate, and the FWHM of this narrow-bandwidth

MA was calculated by simulation up to 0.38 nm[18].

Although the design and preparation of narrow-bandwidth MAs using dielectric materials can reduce fabrication costs and improve absorption efficiency, and the absorption bandwidth can be maintained at the sub-nanometer level, it can be seen that few MAs that achieve multi-wavelength narrow-bandwidth (sub-nanometer level) absorption are currently available. This can limit the application of narrow-bandwidth MAs in some applications, such as in spectral detection and gas detection, where multi-wavelength narrow-bandwidth MAs are more efficient in improving their efficiency[19-20]. To this end, a dual-wavelength narrow-bandwidth dielectric MA consisting of an asymmetric dielectric grating, a dielectric transition layer, and a metal substrate is proposed in this paper, and the MA is designed and analyzed using the Finite Difference Time Domain (FDTD) method. The differential form of Maxwell's equations can be numerically solved in the time domain through FDTD, in which the differential quotient can be substituted for the differential in the equation. In the solution, the electric and magnetic fields are alternately distributed, and the electric and magnetic fields in the simulation region are solved over time. Through simulation calculations, it is found that the FWHM of the dual-wavelength narrow-bandwidth MA is as low as 0.077 nm and the quality factor (figure of merit, FOM) is up to 1 524/RIU, and it can also be found that the narrowest absorption bandwidth of the narrow-bandwidth MA designed in this paper decreased by an order of magnitude compared to the reference [14-18]. This study can provide high-quality dual-wavelength narrow-bandwidth dielectric MAs for biosensors, thermal emitters, light modulators, etc.

2　Device structure

A dual-wavelength narrow-bandwidth dielectric MA, as shown in Figure 1, consists of an Au substrate, a silicon dioxide (SiO_2) dielectric layer, and an asymmetric grating formed by silicon (Si) material from the bottom up. The main function of the Au substrate is to suppress light transmission, so its thickness must be greater than the skinning depth of the incident electromagnetic wave, and the thickness of Au is set to 0.2 μm in this paper. It can be seen from Figure 1 that there are two gratings with the same height h but different widths, W_1 and W_2, in a period, and the distance between the gratings in the same period is g, and the thickness of SiO_2 is t. In the future practical device preparation, the preparation process of the dual-wavelength narrow-bandwidth dielectric MA in this paper is compatible with the current micro-nano processing process. First, SiO_2 and Si thin layers are grown successively on the Au substrate by magnetron sputtering, followed by spin-coating electron beam resist on the Si thin layer, forming asymmetric grating patterns on the resist after electron beam exposure and development, and then debonding and transferring the patterns to the Si thin layer using inductively coupled plasma etching to finally prepare the dual-wavelength narrow-bandwidth dielectric MA[21].

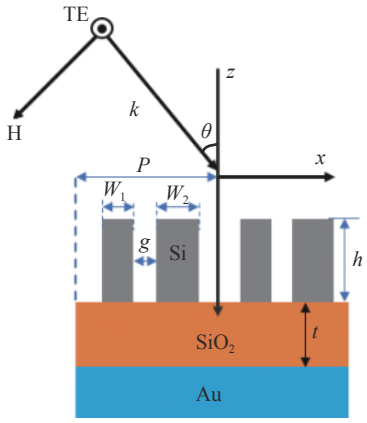

Fig. 1　Dual-wavelength narrow-bandwidth dielectric MA structure diagram

图 1　双波长窄带宽介质 MA 结构图

The dielectric constant of Au is represented by the Drude model as shown in Equation (1), where ω_p, γ and ω are the plasma frequency, damping coefficient and incident light angle frequency, re-

spectively. To ensure the correctness of the simulation calculation results, ω_p and γ are obtained from the experimental data, and according to the reference [22], ω_p=1.32×10^{16} rad/s, γ=1.2×10^{14} rad/s. The refractive indices of SiO_2 and Si are n_{SiO_2}=1.45 and n_{Si}=3.45, respectively.

$$\varepsilon_{Au} = 1 - \frac{\omega_p^2}{\omega^2 + i\gamma\omega} \quad . \qquad (1)$$

3 Results and discussion

3.1 Realization of dual-wavelength narrow-bandwidth and high absorption

Firstly, a two-dimensional physical model of a single period of the dual-wavelength narrow-bandwidth dielectric MA is established using FDTD, and then periodic boundary conditions are added in the x-direction, perfect matching layer boundary conditions are added in the z-direction, and the y-direction is set to grating infinite length by default. Finally, a light source is added directly above the dual-wavelength narrow-bandwidth dielectric MA, the light source polarization is set to TE polarization, the incident angle is set to 0°, and the MA is surrounded by air with refractive index n=1.

Figure 2 shows the absorption spectrum of the dual-wavelength narrow-bandwidth dielectric MA, where P=1.05 μm, t=1.2 μm, h=0.78 μm, W_1=0.2 μm, W_2=0.3 μm and g=0.2 μm. The above grating parameters were obtained based on FDTD optimization. It can be seen from the figure that the MA has ultra-high absorption efficiency at wavelengths λ_1=1.208 5 μm and λ_2=1.238 2 μm, respectively, and the absorption linewidths FWHM are 0.735 nm and 0.077 nm, respectively. By comparing with references [14-15, 17], the linewidth of the dual-wavelength narrow-bandwidth dielectric MA at wavelength λ_2 is significantly decreased and narrow-bandwidth absorption is achieved. All parameters mentioned above were kept constant for subsequent calculations if not otherwise stated.

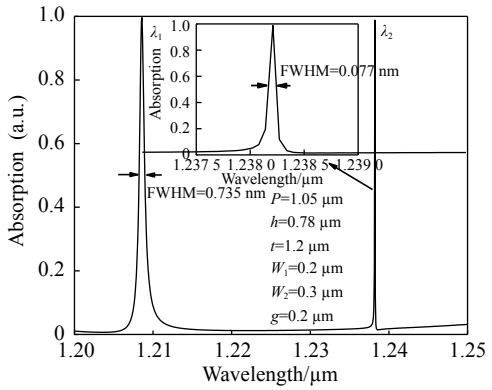

Fig. 2 Absorption spectroscopy of dual-wavelength narrow-bandwidth dielectric MA

图 2 双波长窄带宽介质 MA 吸收光谱

MA can achieve ultra-narrow bandwidth high absorption at wavelengths λ_1=1.208 5 μm and λ_2=1.238 2 μm because the effective impedance of MA at these two wavelengths just matches the free-space impedance and thus the reflection of MA at wavelengths λ_1 and λ_2 can be effectively suppressed[23]. Because the absorption efficiency A of MA can be expressed as A=1-T-R, because the thickness of Au substrate is greater than the skinning depth of light, so T=0, and when the reflection of MA at wavelengths λ_1 and λ_2 is suppressed, the absorption efficiency of MA at these two wavelengths can be close to 1. The effective impedance Z of MA can be expressed by Equation (2), where S_{11} and S_{21} are the scattering matrix coefficients of reflection and transmission under vertical irradiation of TE polarized light, respectively, and R=$(S_{11})^2$, T=$(S_{21})^2$, and since T=0, S_{21}=0. Figure 3 shows the effective impedance of MA calculated by Equation (2).

From Figure 3(a), it can be seen that the real part of impedance Z_{real} is close to 1 at wavelengths λ_1 and λ_2, while from Figure 3(b) it can be found that the imaginary part of impedance Z_{imag} is close to 0 at wavelengths λ_1 and λ_2.

$$Z = \frac{\sqrt{(1+S_{11})^2 - S_{21}^2}}{\sqrt{(1-S_{11})^2 - S_{21}^2}} = \frac{1+S_{11}}{1-S_{11}} \quad . \qquad (2)$$

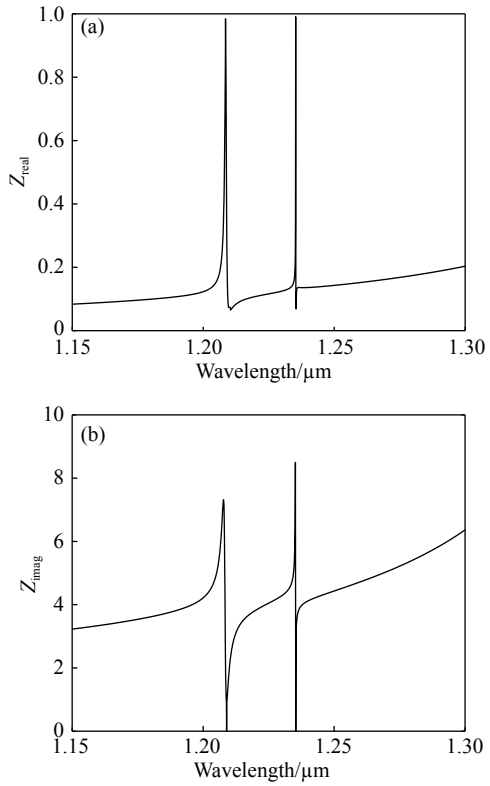

Fig. 3　Effective impedance of dielectric MA. (a) Real part of impedance; (b) imaginary part of impedance

图 3　介质 MA 的有效阻抗。(a)阻抗实部; (b)阻抗虚部

In order to explore the intrinsic physical mechanisms of MA achieving dual-wavelength narrow-bandwidth absorption, the electric field distribution of MA at wavelengths λ_1 and λ_2 respectively, is calculated in this paper, as shown in Figure 4 (Color online). From Figure 4(a), it can be seen that the narrow-bandwidth dielectric MA has high narrow-bandwidth absorption at wavelength λ_1 because most of the light is confined in the SiO_2 dielectric layer, and a small portion of the light is confined in the asymmetric grating. It can be seen that the incident light forms a Fabry-Pérot (FP) cavity resonance in the SiO_2 dielectric layer. Figure 4(b) shows the electric field distribution of the narrow bandwidth dielectric MA at wavelength λ_2. Unlike the electric field distribution at wavelength λ_1, the light is no longer confined in the SiO_2 dielectric layer, but in the grating. Based on the electric field distribution, it can be judged that this is due to the formation of a guided mode resonance in the grating by the incident light[24], which also leads to a narrower bandwidth of the MA at wavelength λ_2.

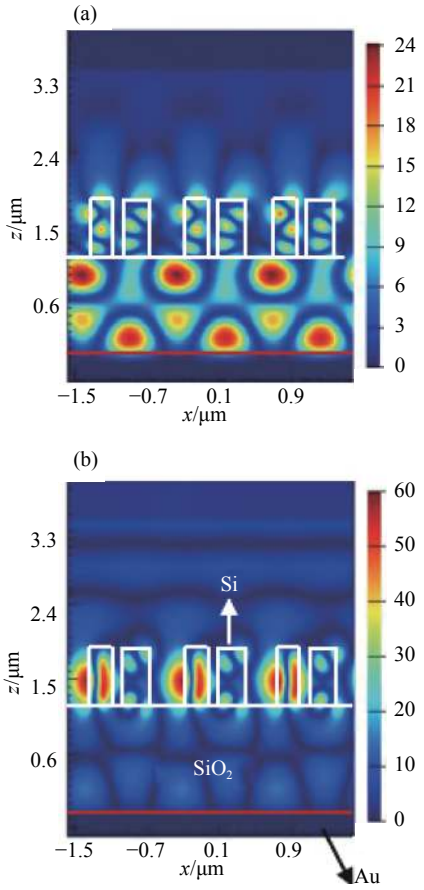

Fig. 4　Electric field distribution of dual-wavelength narrow-bandwidth dielectric MA at different wavelengths. (a) λ_1; (b) λ_2

图 4　双波长窄带宽介质 MA 在不同波长处的电场分布。(a)λ_1; (b)λ_2

3.2　Effect of structural parameters on absorption characteristics of MA

In order to investigate the effect of MA structure parameters on the absorption characteristics of dual-wavelength narrow-bandwidth dielectric, the effect of MA structure parameters on its absorption characteristics is simulated and calculated in this paper. Figure 5 (Color online) shows the effect of different SiO_2 dielectric layer thickness t on MA absorption characteristics. From Figure 5(a), it can be seen that the absorption wavelength λ_1 of MA is redshifted as t increases, however, the change in t has a very weak effect on the absorption wavelength λ_2. From Figure 5(b), it can be seen when t increases

from 1.2 μm to 1.215 μm, the absorption wavelength λ_1 is red-shifted from 1.208 5 μm to 1.211 5 μm, an increase of 3 nm. The change in t has a significant effect on the MA absorption wavelength λ_1, which is due to the FP cavity resonance formed by the light in the SiO_2 dielectric layer as seen in Figure 4(a). The relationship between FP cavity resonance wavelength and SiO_2 layer thickness t is shown in Equation (3)[25],

$$2n_{eq}t + \Phi\lambda_{FP} = N\lambda_{FP} \quad , \qquad (3)$$

where n_{eq} is the equivalent refractive index of FP cavity, Φ is the sum of the phases of the upper and lower interfaces of the FP cavity, and N is an integer, λ_{FP} is the resonant wavelength of the FP cavity. According to Equation (3), it is known that an increase in t increases the FP cavity resonance wavelength λ_{FP} which leads to a red shift in the absorption wavelength λ_1 of MA.

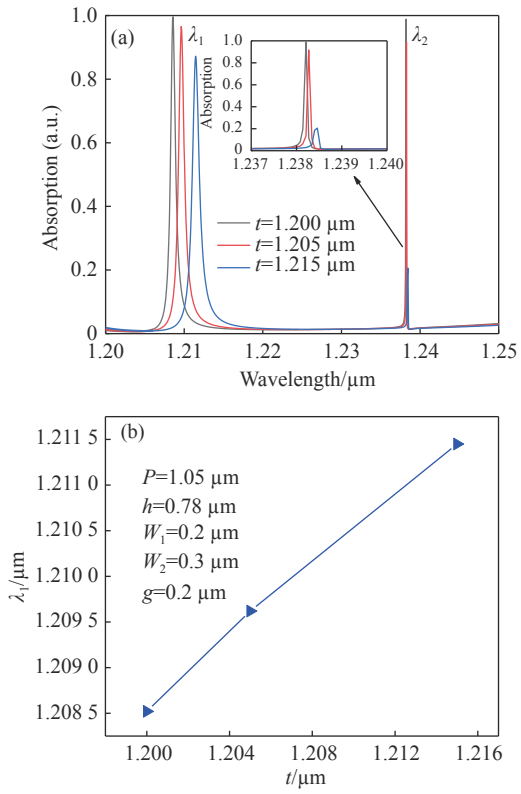

Fig. 5 Effect of t on the absorption characteristics of the dual-wavelength narrow-bandwidth dielectric MA. (a) Absorption spectra; (b) absorption wavelength

图 5 t 对双波长窄带宽介质 MA 吸收特性的影响。(a)吸收光谱;(b)吸收波长

However, the reason why the increase in t has a weaker effect on the absorption wavelength λ_2 of MA is that the narrow-bandwidth and high-absorption of MA at wavelength λ_2 are caused by guided mode resonance, which can be seen from Figure 4(b). According to Ref. [26], the guided mode resonance wavelength is mainly related to the grating parameters and the incident angle. However, the absorption efficiency of MA at the absorption wavelength λ_2 will gradually decrease as t increases, which can be explained by Figure 6 (Color online). Figure 6 is the electric field distribution of MA at wavelength λ_2 when t=1.205 μm. Comparing Figure 6 with Figure 4(b), it can be found that the electric field focused in the grating in Figure 6 is significantly lower than Figure 4(b). Therefore, the absorption rate of MA will decrease after t becomes larger.

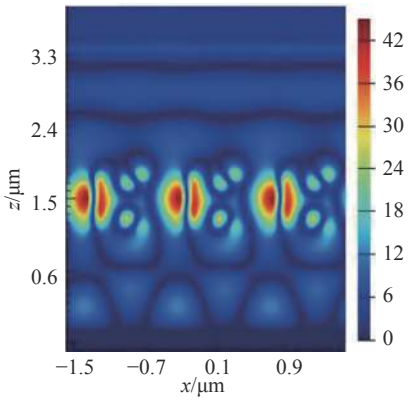

Fig. 6 Electric field distribution of MA at wavelength λ_2 when t = 1.205 μm

图 6 t=1.205 μm 时 MA 在波长 λ_2 处的电场分布

Figure 7 (Color online) shows the effect of grating width W_1 on the absorption characteristics of dual-wavelength narrow-bandwidth dielectric MA. It can be seen from Figure 7(a) that the absorption wavelengths λ_1 and λ_2 of MA both have red shifted as W_1 becomes larger, respectively. It can be seen from Figure 7(b) that when W_1 increases from 0.2 μm to 0.202 μm, the absorption wavelength λ_2 of MA is red-shifted by nearly 7 nm, while the absorption wavelength λ_1 of MA is red-shifted by 1.46 nm.

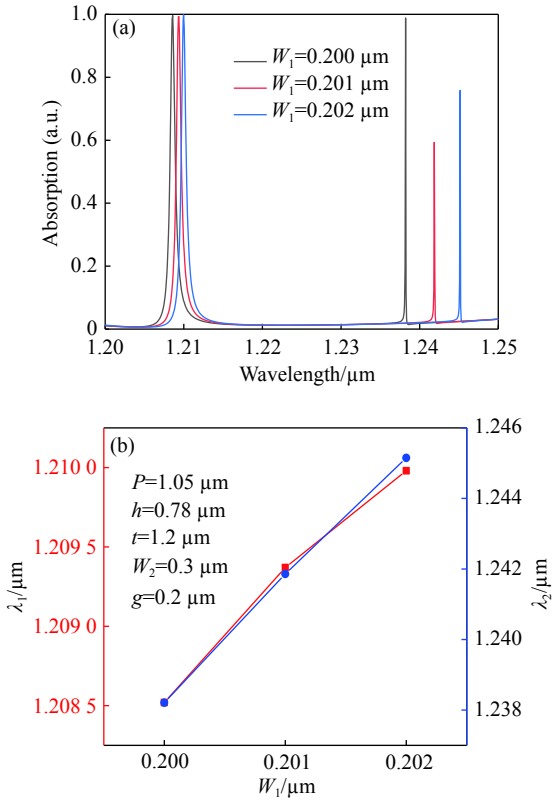

Fig. 7　Effect of W_1 on the absorption characteristics of the dual-wavelength narrow-bandwidth dielectric MA. (a) Absorption spectra; (b) absorption wavelength

图 7　W_1 对双波长窄带宽介质 MA 吸收特性的影响。(a) 吸收光谱; (b)吸收波长

The change of W_1 can have an impact on the absorption wavelength λ_1 because it can be known that the change of the grating width will lead to a change in the equivalent refractive index of the asymmetric grating, and the equivalent refractive index of the FP cavity n_{eq} is effectd by the equivalent refractive index of the asymmetric grating n_w. Moreover, it has been shown in Ref. [27] that the increase of the grating width will lead to the increase of the equivalent refractive index of the FP cavity n_{eq}. From Equation (3), it is known that an increase in n_{eq} will increase the FP cavity resonance wavelength λ_{FP}. And the increase of λ_{FP} will lead to the red-shift of the absorption wavelength λ_1 of MA. Figure 8 shows n_{eq} varying with W_1 and it is calculated by FDTD. From Figure 8, it can be found that when W_1 increases from 0.2 μm to 0.202 μm, n_{eq} increases from 1.510 to 1.512.

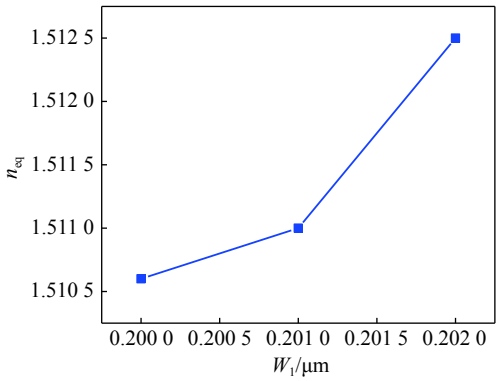

Fig. 8　Effect of W_1 on n_{eq}

图 8　W_1 对 n_{eq} 的影响

The grating, SiO_2 layer, and air form an optical waveguide, and according to the grating guided-mode resonance theory, it is known that the grating equivalent refractive index change will affect the guided-mode resonance wavelength[26], as shown in Equation (4).

$$n_w = n\sin\theta + m\frac{\lambda_g}{P} \quad . \qquad (4)$$

where λ_g is the guided-mode resonance wavelength and m is the diffraction order of the grating. According to the equivalent medium theory, an increase in W_1 will increase the grating equivalent refractive index n_w, and from Eq. (4), an increase in n_w will red-shift the guided-mode resonance wavelength λ_g and thus the MA absorption wavelength λ_2 will red-shift. The effect of W_2 on MA absorption characteristics is not shown in this paper, because the effect of the change in W_2 on MA absorption characteristics is similar to that of W_1 on MA, and the intrinsic physical mechanism of the effect is essentially the same.

The electric field distribution in Figure 4(b) shows that a part of the electric field is distributed among the slits of the dielectric grating, so it can be seen that the change of the surrounding gas will have an effect on the absorption wavelength λ_2 of MA. Therefore, the narrow bandwidth dielectric MA proposed in this paper can be applied in the fields of gas or biological detection. In order to evaluate the performance of the narrow-bandwidth dielectric MA in gas detection, two parameters,

sensitivity and quality factor, are defined, and the specific expressions are shown in equations (5) and (6). Where S is the sensitivity of narrow-bandwidth MA, $\triangle n$ and $\triangle \lambda$ are the amount of change in refractive index and the amount of change in absorption wavelength of the surrounding gas, respectively[18].

$$S = \frac{\Delta\lambda}{\Delta n} \quad , \tag{5}$$

$$FOM = \frac{S}{FWHM} \quad . \tag{6}$$

From Figure 9 (a) (Color online), it can be seen that the absorption wavelengths λ_1 and λ_2 of MA are redshifted as n increases. This is because a larger n leads to a larger refractive index n_l of the grating's low refractive index material, which in turn leads to a larger equivalent refractive index of the grating for different wavelengths. And from the previous description, the grating refractive index will lead to a larger equivalent refractive index n_{eq} of FP cavity, so according to Equation (3), the increase of n will lead to a red shift of MA absorption wavelength λ_1. Unlike the mechanism that causes the red shift of MA absorption wavelength λ_1, λ_2 is red-shifted as n becomes larger, because the grating equivalent refractive index n_w increases, which means that it increases the refractive index of the central layer of the optical waveguide, and this must lead to the red shift of the grating guided mode resonance wavelength according to the guided mode resonance theory and Equation (4)[27].

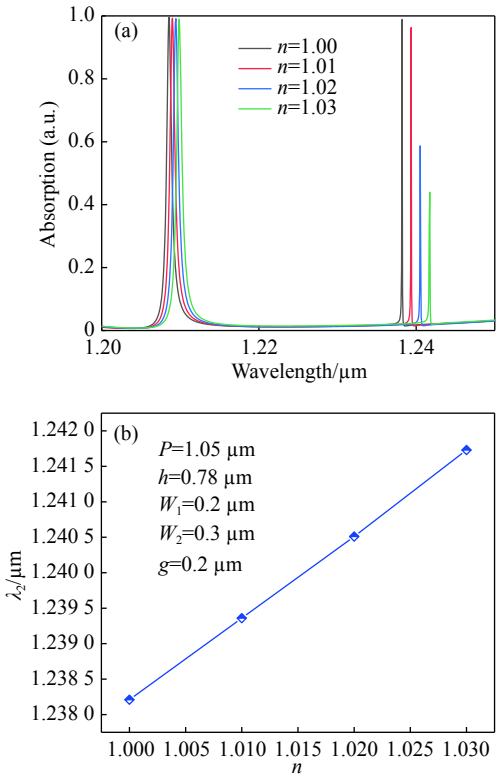

Fig. 9 Effect of n on the absorption characteristics of the dual-wavelength narrow-bandwidth dielectric MA. (a) Absorption spectra; (b) absorption wavelength

图 9 n 对双波长窄带宽介质 MA 吸收特性的影响。(a) 吸收光谱; (b)吸收波长

From Figure 9(b), when n increases from 1 to 1.03, the absorption wavelength λ_2 increases from 1.2382 μm to 1.2417 μm, which is red-shifted by 3.5 nm, and according to Eqs. (5) and (6), S= 117.3 nm/RIU and FOM = 1524/RIU. It can be found that the FOM in this paper is significantly improved compared to the references [14-15, 18].

Finally, the effect of the asymmetric grating period P on the absorption characteristics of the dielectric MA was analyzed, and the specific results are shown in Figure 10 (Color online). From Figure 10, it can be found that the absorption wavelengths λ_1 and λ_2 of MA are red-shifted with the increase of P. When P increases from 1.05 μm to 1.1 μm, the wavelength λ_1 increases from 1.2085 μm to 1.2249 μm, while the wavelength λ_2 increases from 1.2382 μm to 1.2525 μm. From Equation (4) we can know the reason why the wavelength λ_2 increases with the increase of P[24]. When the period increases, if the guided mode resonance is to be maintained, the resonance wavelength must be shifted to the long wavelength direction.

As P increases, the phase Φ of the FP cavity decreases significantly because the effect of the change of P on n_{eq} is not as significant as the phase Φ. Therefore, according to Equation (3), it is known that the FP cavity resonance wavelength λ_{FP} in-

creases with the increase of P, which leads to the red-shift of the absorption wavelength λ_1 of MA. The trend of the effect of P on the phase Φ is calculated by FDTD and is shown in Figure 11, from which it can be seen that Φ decreases from 4.64 rad to 0.22 rad when P increases from 1.05 μm to 1.1 μm.

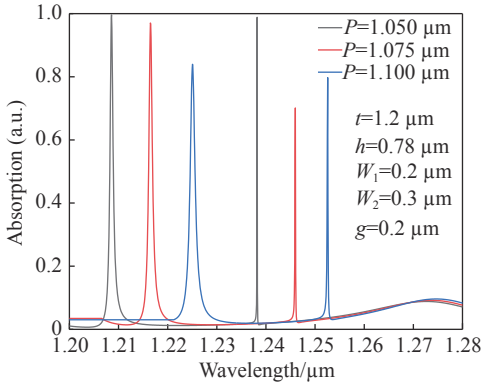

Fig. 10　Effect of P on the absorption characteristics of the dual-wavelength narrow-bandwidth dielectric MA

图 10　P 对双波长窄带宽介质 MA 吸收特性的影响

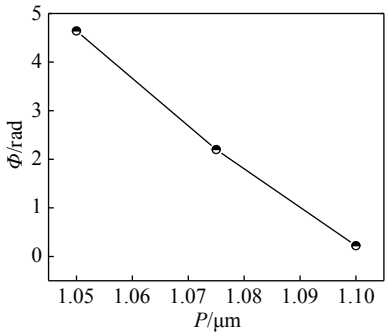

Fig. 11　Effect of P on Φ

图 11　P 对 Φ 的影响

4　Conclusion

In order to broaden the application field of narrow-bandwidth MA, a medium MA is designed in this paper that can achieve dual-wavelength narrow-bandwidth absorption in the infrared band based on the finite-difference time-domain method. Through simulation analysis, the narrow bandwidth dielectric MA in this paper has ultra-high absorption efficiency at wavelength λ_1 = 1.208 5 μm and λ_2 = 1.238 2 μm, and the FWHM is only 0.735 nm and 0.077 nm, respectively. Because of the different mechanisms of MA forming narrow-bandwidth and high absorption on λ_1 and λ_2, the study found that λ_1 is very sensitive to the change of the thickness t of the SiO_2 transition layer, while λ_2 is very sensitive to the change of the dielectric grating width W_1. With the increase of t and W_1, the absorption wavelengths λ_1 and λ_2 of MA will red-shift respectively. When the grating period P increases, the absorption wavelengths λ_1 and λ_2 of MA will shift to the long wavelength direction at the same time. From the electric field distribution of MA at λ_2, a large part of its electric field is distributed in the gap between the gratings, so the change of air refractive index has a significant effect on λ_2. This allows it to be used in the field of detection. It is calculated that the FOM of the narrow-bandwidth dielectric MA in this paper can reach 1 524/RIU.

——中文对照版——

1　引　言

在许多应用中都有需要对电磁波实现完美吸收，如太阳能电池、热发射器、辐射冷却、通信等[1-4]。但是由自然界存在的材料构成的吸收器因缺乏磁响应导致阻抗失配，因此它们不能完全抑制光反射，从而降低了吸收器光吸收能力[5]。因此，人们提出了基于超材料的吸收器，由于超材料吸收器（Metamaterial Absorber, MA）对电磁波具有高吸收效率，且具有体积小、可设定工作波长等优点，逐渐被人们所关注并成为研究热点之一[6]。

经深入研究，人们设计并制备出了不同类型的 MA，如宽带宽 MA、窄带宽 MA、太赫兹 MA、可调谐 MA 等[7-9]。窄带宽 MA 被人们所关注是因为窄带宽 MA 用在探测和热发射器上时相比于宽带宽 MA 效率更高[10-11]，而且在光调制、光探

测和热辐射剪裁中只有窄带宽 MA 才能满足要求[12-13]。目前已经有不同结构的窄带宽 MA 被提出，如基于裂环谐振器阵列（Split Ring Resonator, SRR）、金属/介质周期光栅、金属/介质狭缝（narrow slits）等。2014 年瑞典皇家理工学院的 Min-Qiu 等人提出在银（Ag）金属衬底上刻蚀金属光栅，基于 Ag 光栅与空气介质形成的表面等离子激元共振成功使 MA 在波长 1400 nm 处实现了窄带宽吸收，其线宽（Full Width Half Maximum, FWHM）可以达到 0.4 nm[14]；2018 年香港中文大学的 FENG A 等人提出一种由非对称金属光栅和金属衬底构成的窄带宽 MA，而且在光栅和衬底之间添加了一层二氧化硅过渡层，经模拟计算发现该窄带宽 MA 在光通信波段实现了超窄吸收，FWHM 仅有 0.28 nm[15]；2019 年，东南大学 KANG S 等人提出在二氧化硅衬底上刻蚀出由金（Au）材料构成的十字型纳米阵列，与此同时在二氧化硅另一面生长一层 Au 薄层抑制透射，经测试发现该 MA 可在太赫兹波段实现窄带宽吸收[16]。

从以上研究可以发现，这些窄带宽 MA 中的微纳结构所使用的材料都是金属材料，但是金属材料存在欧姆损耗，而且在高频处精细金属材料存在加工问题，这会在一定程度上影响 MA 在将来的应用推广。因此，一些课题组提出利用介质材料设计、制造窄带宽 MA。2019 年哈尔滨工业大学的 Zhibin Ren 等人利用氮化硅、氧化铟锡材料设计并制备出在红外波段具有窄带宽吸收的 MA，经测试可得该窄带宽 MA 的 FWHM 可达 2.6 nm[17]；2020 年，安徽大学的 Yan Zhao 等人提出在金属衬底上直接刻蚀出由硅材料构成的介质光栅，经模拟计算可知该窄带宽 MA 的 FWHM 可达 0.38 nm[18]。

虽然利用介质材料设计制备窄带宽 MA 可以降低制造成本，提高吸收效率，而且吸收带宽可保持在亚纳米级别，但目前鲜有实现多波长窄带宽亚纳米级别吸收的 MA，这会限制窄带宽 MA 在一些场合的应用，如在光谱探测、气体探测中，多波长窄带宽 MA 更能提高它们的工作效率[19-20]。针对上述需求，本文提出由非对称介质光栅、介质过渡层、金属衬底构成的双波长窄带宽介质 MA，并利用时域有限差分法 (Finite Difference Time Domain, FDTD) 对该 MA 进行设计和分析。FDTD 在时域中对麦克斯韦方程组的微分形式进行数值求解，以差商代替方程中的微分。在求解时电场与磁场交替分布，随着时间的推移求解出仿真区域的电场和磁场。经模拟计算发现双波长窄带宽 MA 的 FWHM 最低可达 0.077 nm，品质因素（Figure Of Merit, FOM）可达 1524/RIU，而且经对比可以发现本文设计的窄带宽 MA 最窄的吸收带宽相比文献 [14-18] 都下降了一个数量级。本文研究可为生物传感器、热发射器、光调制器等提供高质量的双波长窄带宽介质 MA。

2 器件结构

图 1 是双波长窄带宽介质 MA 结构图，它自下而上由 Au 衬底、二氧化硅（SiO_2）介质层、硅（Si）材料形成的非对称光栅组成。Au 衬底的主要作用是抑制光的透射，因此它的厚度必须大于入射电磁波的趋肤深度，本实验中 Au 的厚度设为 0.2 μm。从图 1 中可以看到，一个周期内具有两个同高度（h）、不同宽度的光栅，它们的宽度分别是 W_1 和 W_2，同周期内光栅之间的间距为 g，另外 SiO_2 的厚度为 t。在将来实际器件制备中，本文的双波长窄带宽介质 MA 的制备工艺与现今的微纳加工工艺兼容，通过磁控溅射在 Au 衬底上先后生长 SiO_2 和 Si 薄层，紧接着在 Si 薄层上旋涂电子束抗蚀胶，经电子束曝光和显影后在抗蚀胶上形成非对称光栅图形，去胶并利用感应耦合等离子体刻蚀技术，将图形转移到 Si 薄层上，最终制备出双波长窄带宽介质 MA[21]。

Au 的介质常数由 Drude 模型表示，即

$$\varepsilon_{\mathrm{Au}} = 1 - \frac{\omega_p^2}{\omega^2 + \mathrm{i}\gamma\omega} \quad . \tag{1}$$

式中 ω_p、γ 和 ω 分别是等离子体频率、阻尼系数和入射光角频率。为了保证模拟计算结果正确，ω_p 和 γ 均是从实验数据中获得，根据文献 [22] 可知，ω_p=1.32×10^{16} rad/s，γ=1.2×10^{14} rad/s。SiO_2 和 Si 的折射率分别为$n_{\mathrm{SiO_2}}$=1.45 和n_{Si}=3.45。

3 结果与讨论

3.1 双波长窄带宽高吸收的实现

首先利用 FDTD 软件建立双波长窄带宽介质 MA 单个周期的二维物理模型，然后在 x 方向

添加周期性边界条件，在 z 方向添加完美匹配层边界条件，y 方向默认为光栅无限长。最后在双波长窄带宽介质 MA 正上方添加光源，光源偏振设为 TE 偏振，入射角设为 0°，并且 MA 周围为空气，折射率 n=1。

图 2 所示的是双波长窄带宽介质 MA 的吸收光谱，此时 P=1.05 μm、t=1.2 μm、h=0.78 μm、W_1=0.2 μm、W_2=0.3 μm、g=0.2 μm，上述光栅参数是基于 FDTD 优化后获得的。从图 2 中可以看到 MA 分别在波长 λ_1=1.208 5 μm 和 λ_2=1.238 2 μm 处具有超高吸收效率，吸收线宽 FWHM 分别为 0.735 nm 和 0.077 nm。相比于文献 [14-15, 17] 结果，双波长窄带宽介质 MA 在波长 λ_2 处的线宽明显下降，实现了窄带宽吸收。若无特殊说明，上述所有参数保持不变。

MA 能在波长 λ_1=1.208 5 μm 和 λ_2=1.238 2 μm 实现超窄带宽高吸收，是因为 MA 在这两个波长处的有效阻抗刚好与自由空间阻抗相匹配，这可有效地抑制 MA 对波长 λ_1 和 λ_2 的反射[23]。因为 MA 的吸收效率 A 可表示为 A=1-T-R，由于 Au 衬底的厚度大于光的趋肤深度，所以 T=0，而当 MA 在波长 λ_1 和 λ_2 的反射得到抑制后，MA 对这两个波长的吸收效率就接近 1。MA 的有效阻抗 Z 可由式(2)表示：

$$Z=\frac{\sqrt{(1+S_{11})^2-S_{21}^2}}{\sqrt{(1-S_{11})^2-S_{21}^2}}=\frac{1+S_{11}}{1-S_{11}} \quad . \qquad (2)$$

式中 S_{11} 和 S_{21} 分别是 TE 偏振光垂直照射下反射和透射的散射矩阵系数，其中 R=$(S_{11})^2$,T=$(S_{21})^2$，由于 T=0，所以 S_{21}=0。图 3 是由式(2)计算得到的 MA 的有效阻抗，从图 3(a)中可知阻抗的实部 Z_{real} 在波长 λ_1 和 λ_2 处接近为 1，而从图 3(b)中可以发现阻抗的虚部 Z_{imag} 在波长 λ_1 和 λ_2 接近为 0。

为了探索 MA 实现双波长窄带宽吸收的内在物理机制，本文计算了 MA 分别在波长 λ_1 和 λ_2 处的电场分布，具体如图 4(彩图见期刊电子版)所示。从图 4(a)中可知，窄带宽介质 MA 之所以在波长 λ_1 出现窄带宽高吸收是因为大部分光被限制在 SiO_2 介质层当中，少部分光限制在非对称光栅当中。由此可知，入射光在 SiO_2 介质层当中形成了法布里-珀罗 (Fabry-Pérot, FP) 腔共振。图 4(b)所示的是窄带宽介质 MA 在波长 λ_2 的电场分布，与在波长 λ_1 的电场分布不同，此时光不再被限制在 SiO_2 介质层当中，反而是被限制在光栅当中，依据电场分布可以判断这是由于入射光在光栅中形成了导模共振[24]，也因为导模共振导致 MA 在波长 λ_2 处的带宽更窄。

3.2　结构参数对 MA 吸收特性的影响

为了探究双波长窄带宽介质 MA 结构参数对其吸收特性的影响规律，本文模拟计算了 MA 结构参数对其吸收特性的影响。图 5(彩图见期刊电子版)是不同 SiO_2 介质层厚度 t 对 MA 吸收特性的影响。从图 5(a)中可知，随着 t 的增加，MA 的吸收波长 λ_1 会出现红移现象，但是 t 的变化对吸收波长 λ_2 的影响非常微弱。由图 5(b)可得，当 t 从 1.2 μm 增加到 1.215 μm，吸收波长 λ_1 从 1.208 5 μm 红移到 1.211 5 μm，增加了 3 nm。t 的变化能够对 MA 吸收波长 λ_1 有显著影响，是因为由图 4(a)可知光在 SiO_2 介质层中形成了 FP 腔共振。FP 腔共振波长与 SiO_2 层厚度 t 的关系为[25]：

$$2n_{\text{eq}}t+\Phi\lambda_{\text{FP}}=N\lambda_{\text{FP}} \quad , \qquad (3)$$

式中，n_{eq} 是 FP 腔的等效折射率，Φ 是 FP 腔上下界面相位之和，N 是整数，λ_{FP} 是 FP 腔共振波长。根据式(3)可知 t 增大会导致 FP 腔共振波长 λ_{FP} 增大，从而导致 MA 的吸收波长 λ_1 出现红移现象。

由图 4(b)可知，MA 在波长 λ_2 处实现窄带宽高吸收是因为导模共振效应，而根据文献 [26] 可知，导模共振波长主要与光栅参数、入射角等有关。但是可以发现随着 t 的增大，MA 在吸收波长 λ_2 的吸收效率会逐渐下降，这可由图 6(彩图见期刊电子版)解释。图 6 是 t=1.205 μm 时 MA 在波长 λ_2 处电场分布，将图 6与图 4(b)相比，可以发现在图 6 中聚集在光栅中的电场明显低于图 4(b)，故此导致 MA 在 t 变大后的吸收率会下降。

图 7(彩图见期刊电子版)所示的是光栅宽度 W_1 对双波长窄带宽介质 MA 吸收特性的影响。由图 7(a)可知，随着 W_1 的变宽，MA 的吸收波长 λ_1 和 λ_2 都分别出现了红移现象。从图 7(b)可知，当 W_1 从 0.2 μm 增加到 0.202 μm，MA 的吸收波长 λ_2 红移了将近 7 nm，而 MA 的吸收波长 λ_1 红移了 1.46 nm。

W_1 的变化能够对吸收波长 λ_1 产生影响是因为根据等效介质原理可知光栅宽度的变化会导致

非对称光栅的等效折射率发生变化，而 FP 腔的等效折射率 n_{eq} 又受非对称光栅等效折射率 n_w 的影响。而且文献 [27] 也已经证明，光栅宽度增加会导致 FP 腔等效折射率 n_{eq} 增大，由式(3)可知，n_{eq} 增大，FP 腔共振波长 λ_{FP} 也将会增大。λ_{FP} 增大就会导致 MA 的吸收波长 λ_1 红移。图 8 是当 W_1 取不同值时 n_{eq} 的变化情况，它是由 FDTD 计算获得。从图 8 中可以发现，当 W_1 从 0.2 μm 增加到 0.202 μm，n_{eq} 则从 1.510 增加到 1.512.

光栅、SiO_2 层、空气形成了光波导，根据光栅导模共振理论可知，光栅等效折射率的改变将会影响导模共振波长[26]，即

$$n_w = n\sin\theta + m\frac{\lambda_g}{P} \quad . \tag{4}$$

式中 λ_g 是导模共振波长，m 为光栅的衍射阶数。由等效介质理论可知，W_1 增大将会使光栅等效折射率 n_w 增大，而根据式(4)可知，n_w 增大则使导模共振波长 λ_g 红移，从而使 MA 吸收波长 λ_2 红移。在本文中之所以没有展示 W_2 对 MA 吸收特性的影响，是因为 W_2 的变化对 MA 吸收特性的影响与 W_1 对 MA 的影响相似，而且内在物理机理也基本相同。

通过图 4(b)的电场分布可知，有一部分电场分布在介质光栅缝隙中，由此可知，周围气体的变化将会对 MA 的吸收波长 λ_2 产生影响，因此本文提出的窄带宽介质 MA 可应用在气体或生物探测等领域当中。为了评估窄带宽介质 MA 在气体探测中的工作性能，定义了灵敏度和品质因素两个参数，即

$$S = \frac{\Delta\lambda}{\Delta n} \quad , \tag{5}$$

$$FOM = \frac{S}{FWHM} \quad , \tag{6}$$

式中 S 是窄带宽 MA 的灵敏度，$\triangle n$ 和 $\triangle\lambda$ 分别是周围气体折射率的变化量和吸收波长的变化量[18]。

从图 9(a)(彩图见期刊电子版)可知，随着 n 的增加，MA 的吸收波长 λ_1 和 λ_2 都出现了红移的现象。因为 n 变大会导致光栅低折射率材料折射率 n_l 变大，而 n_l 变大又会导致光栅对不同波长的等效折射率变大。而由前面所述可知，光栅折射率变大会导致 FP 腔等效折射率 n_{eq} 变大，所以根据式(3)可知，n 的增加会导致 MA 吸收波长 λ_1 红移。与导致 MA 吸收波长 λ_1 红移的机理不同，MA 吸收波长 λ_2 之所以会随着 n 变大而红移，是因为其增大了光栅等效折射率 n_w，这意味着增大了光波导中心层的折射率，而根据导模共振理论和式(4)可知[27]，这必定会导致光栅导模共振波长的红移。

从图 9(b)可知，当 n 从 1 增加到 1.03，吸收波长 λ_2 会从 1.2382 μm 增加到 1.2417 μm，红移了 3.5 nm，根据式(5)和式(6)可得，S=117.3 nm/RIU，FOM=1524/RIU。本文的FOM 相比文献[14-15,18]有了明显提高。

最后分析了非对称光栅周期 P 对介质 MA 吸收特性的影响，具体结果如图 10(彩图见期刊电子版)所示。从图 10 中可以发现，随着 P 的增加，MA 的吸收波长 λ_1 和 λ_2 都产生了红移现象。当 P 从 1.05 μm 增加到 1.1 μm 后，波长 λ_1 则从 1.2085 μm 增加到了 1.2249 μm，而波长 λ_2 则从 1.2382 μm 增加到了 1.2525 μm。由式(4)可知，波长 λ_2 之所以会随着 P 的增大而增大[24]，是因为周期增大时若要维持导模共振，则必须使得共振波长向长波长方向移动。

随着 P 的增加 FP 腔的相位 Φ 会显著下降，因为 P 的变化对 n_{eq} 的影响并无相位 Φ 的显著，所以根据式(3)可知，随着 P 的增加 FP 腔共振波长 λ_{FP} 会增大，从而导致 MA 的吸收波长 λ_1 出现红移现象。P 对相位 Φ 的影响趋势如图 11 所示，该结果由 FDTD 计算得到，从图 11 中可知当 P 从 1.05 μm 增大到 1.1 μm，Φ 会从 4.64 rad 下降到 0.22 rad。

4 结 论

为了拓宽窄带宽 MA 的应用领域，本文基于时域有限差分法设计了在红外波段上可实现双波长窄带宽吸收的介质 MA，经模拟分析发现，本文的窄带宽介质 MA 在波长 λ_1=1.2085 μm 和 λ_2=1.2382 μm 具有超高吸收效率，而且 FWHM 也分别只有 0.735 nm 和 0.077 nm。由于 MA 在 λ_1 和 λ_2 上形成窄带宽高吸收的机理不同，所以经本文研究发现，λ_1 对 SiO_2 过渡层的厚度 t 变化非常敏感，但是 λ_2 却对介质光栅宽度 W_1 的变化非常敏感，随着 t 和 W_1 的增加，MA 的吸收波长 λ_1 和 λ_2 都会分别出现红移现象。而当光栅周期 P 增加

时，MA 的吸收波长 λ_1 和 λ_2 会同时向长波长方向偏移。从 MA 在 λ_2 处的电场分布可知，其电场有一大部分是分布在光栅之间的空隙当中，因此空气折射率的变化对 λ_2 有显著影响，这可使其应用在探测领域当中，经计算可得本文的窄带宽介质 MA 的 FOM 可达 1 524/RIU。

References:

[1] 张检发, 袁晓东, 秦石乔. 可调太赫兹与光学超材料[J]. 中国光学, 2014, 7(3): 349-364.
ZHANG J F, YUAN X D, QIN SH Q. Tunable terahertz and optical metamaterials[J]. *Chinese Optics*, 2014, 7(3): 349-364. (in Chinese)

[2] DU K K, LI Q, LV Y B, *et al*.. Control over emissivity of zero-static-power thermal emitters based on phase-changing material GST[J]. *Light*, *Science & Applications*, 2017, 6(1): e16194.

[3] HE X Y, LIU F, LIN F T, *et al*.. Tunable 3D Dirac-semimetals supported mid-IR hybrid plasmonic waveguides[J]. *Optics Letters*, 2021, 46(3): 472-475.

[4] HE X Y, LIU F, LIN F T, *et al*.. Tunable terahertz Dirac semimetal metamaterials[J]. *Journal of Physics D*: *Applied Physics*, 2021, 54(3): 235103.

[5] MOU N L, LIU X L, WEI T, *et al*.. Large-scale, low-cost, broadband and tunable perfect optical absorber based on phase-change material[J]. *Nanoscale*, 2020, 12(9): 5374-5379.

[6] LANDY N I, SAJUYIGBE S, MOCK J J, *et al*.. Perfect metamaterial absorber[J]. *Physical Review Letters*, 2008, 100(20): 207402.

[7] TUAN T S, HOA N T Q. Numerical study of an efficient broadband metamaterial absorber in visible light region[J]. *IEEE Photonics Journal*, 2019, 11(3): 4600810.

[8] PENG J, HE X Y, SHI CH Y Y, *et al*.. Investigation of graphene supported terahertz elliptical metamaterials[J]. *Physica E*: *Low-Dimensional Systems and Nanostructures*, 2020, 124: 114309.

[9] YAO G, LING F R, YUE J, *et al*.. Dual-band tunable perfect metamaterial absorber in the THz range[J]. *Optics Express*, 2016, 24(2): 1518-1527.

[10] LIU N, MESCH M, WEISS T, *et al*.. Infrared perfect absorber and its application as plasmonic sensor[J]. *Nano Letters*, 2010, 10(7): 2342-2348.

[11] GREFFET J J, CARMINATI R, JOULAIN K, *et al*.. Coherent emission of light by thermal sources[J]. *Nature*, 2002, 416(6876): 61-64.

[12] ZHU ZH H, EVANS P G, HAGLUND R F JR, *et al*.. Dynamically reconfigurable metadevice employing nanostructured phase-change materials[J]. *Nano Letters*, 2017, 17(8): 4881-4885.

[13] ANKER J N, HALL W P, LYANDRES O, *et al*.. Biosensing with plasmonic nanosensors[J]. *Nature Materials*, 2008, 7(6): 442-453.

[14] MENG L J, ZHAO D, RUAN ZH C, *et al*.. Optimized grating as an ultra-narrow band absorber or plasmonic sensor[J]. *Optics Letters*, 2014, 39(5): 1137-1140.

[15] FENG A S, YU Z J, SUN X K. Ultranarrow-band metagrating absorbers for sensing and modulation[J]. *Optics Express*, 2018, 26(22): 28197-28205.

[16] KANG S, QIAN ZH Y, RAJARAM V, *et al*.. Ultra-narrowband metamaterial absorbers for high spectral resolution infrared spectroscopy[J]. *Advanced Optical Materials*, 2019, 7(2): 1801236.

[17] RRN ZH B, SUN Y H, LIN Z H, *et al*.. Ultra-narrow band perfect metamaterial absorber based on dielectric-metal periodic configuration[J]. *Optical Materials*, 2019, 89: 308-315.

[18] LIAO Y L, ZHAO Y. Ultra-narrowband dielectric metamaterial absorber with ultra-sparse nanowire grids for sensing applications[J]. *Scientific Reports*, 2020, 10(1): 1480.

[19] XU Z CH, GAO R M, DING CH F, *et al*.. Multiband metamaterial absorber at terahertz frequencies[J]. *Chinese Physics Letters*, 2014, 31(5): 054205.

[20] HU F R, WANG L, QUAN B G, *et al*.. Design of a polarization insensitive multiband terahertz metamaterial absorber[J]. *Journal of Physics D*: *Applied Physics*, 2013, 46(19): 195103.

[21] DING F, DAI J, CHEN Y T, *et al*.. Broadband near-infrared metamaterial absorbers utilizing highly lossy metals[J]. *Scientific Reports*, 2016, 6(1): 39445.

[22] JOHNSON P B, CHRISTY R W. Optical constants of the noble metals[J]. *Physical Review B*, 1972, 6(12): 4370-4379.

[23] LI W CH, ZHOU X, YING Y, *et al*.. Polarization-insensitive wide-angle multiband metamaterial absorber with a

double-layer modified electric ring resonator array[J]. *AIP Advances*, 2015, 5(6): 067151.

[24] 王琦. 导模共振亚波长器件的机理及特性研究[D]. 上海: 上海理工大学, 2012: 44-46.
WANG Q. Study on the mechanism and characteristics of guided-mode resonance subwavelength device[D]. Shanghai: University of Shanghai for Science and Technology, 2012: 44-46. (in Chinese)

[25] 曾志文, 刘海涛, 张斯文. 基于Fabry-Perot模型设计亚波长金属狭缝阵列光学异常透射折射率传感器[J]. *物理学报*, 2012, 61(20): 200701.
ZENG ZH W, LIU H T, ZHANG S W. Design of extraordinary-optical-transimission refractive-index sensor of subwavelength metallic slit array based on a Fabry-Perot model[J]. *Acta Physica Sinica*, 2012, 61(20): 200701. (in Chinese)

[26] 刘文兴. 可控线宽导模共振滤波器设计及其特性研究[D]. 南昌: 南昌大学, 2011: 18-22.
LIU W X. Design and characterization of controllable linewidth guided-mode resonance filter[D]. Nanchang: Nanchang University, 2011: 18-22. (in Chinese)

[27] 江孝伟, 武华. 吸收波长和吸收效率可控的超材料吸收器[J]. *物理学报*, 2021, 70(2): 027804.
JIANG X W, WU H. Metamaterial absorber with controllable absorption wavelength and absorption efficiency[J]. *Acta Physica Sinica*, 2021, 70(2): 027804. (in Chinese)

Author Biographics:

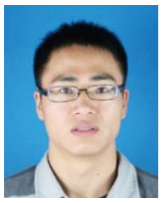

FANG Xiao-min (1985—), male, born in Quzhou, Zhejiang, master, associate professor. In 2010, he received a master's degree from China Jiliang University. His research focuses on metamaterials and optoelectronic devices. E-mail: zhjfangxiaomin@163.com

方晓敏(1985—), 男, 浙江衢州人, 硕士, 副教授, 2010 年于中国计量大学获得硕士学位, 主要从事超材料和光电子器件的研究。E-mail: zhjfangxiaomin@163.com

JIANG Xiao-wei (1991—), male, born in Jiangshan, Zhejiang, master, lecturer. He received his master's degree from Beijing Institute of Technology in 2016, and since then he has focused on metamaterials and optoelectronic devices. Email: JosephJiangquzhi@126.com

江孝伟(1991—), 男, 浙江江山人, 硕士, 讲师, 2016 年于北京工业大学获得硕士学位, 主要从事超材料和光电子器件的研究。Email: JosephJiangquzhi@126.com

WU Hua (1980—), male, from Xiantao, Hubei, Ph.D., associate professor. After obtaining master's and doctoral degrees from Guangdong University of Technology and Beijing University of Technology in 2006 and 2015, he is mainly engaged in the research of micro-nano materials and semiconductor optoelectronic devices. Email: wh1125@126.com

武 华(1980—), 男, 湖北仙桃人, 博士, 副教授, 2006 年于广东工业大学获得硕士学位, 2015 年于北京工业大学获得博士学位, 主要从事微纳材料和半导体光电子器件的研究。Email: wh1125@126.com